J. Fluid Mech. (2011), *vol.* 682, *pp.* 213–240. © Cambridge University Press 2011
doi:10.1017/jfm.2011.211

Dissipation in rapid dynamic wetting

A. CARLSON†‡, M. DO-QUANG AND G. AMBERG

Linné Flow Center, Department of Mechanics, The Royal Institute of Technology, SE-100 44, Stockholm, Sweden

(Received 16 March 2010; revised 13 December 2010; accepted 8 May 2011; first published online 24 June 2011)

In this article, we present a modelling approach for rapid dynamic wetting based on the phase field theory. We show that in order to model this accurately, it is important to allow for a non-equilibrium wetting boundary condition. Using a condition of this type, we obtain a direct match with experimental results reported in the literature for rapid spreading of liquid droplets on dry surfaces. By extracting the dissipation of energy and the rate of change of kinetic energy in the flow simulation, we identify a new wetting regime during the rapid phase of spreading. This is characterized by the main dissipation to be due to a re-organization of molecules at the contact line, in a diffusive or active process. This regime serves as an addition to the other wetting regimes that have previously been reported in the literature.

Key words: contact lines, drops, interfacial flows (free surface)

1. Introduction

Contact lines between solids and liquid or gas interfaces appear in very many instances of fluid flows. This could be coffee stains, water–oil mixtures in oil recovery, hydrophobic feet of insects or surfaces of leaves in nature. Due to their ubiquitous occurrence in nature and our daily life, as well as in industrial processes, they have attracted the attention of researchers since many years. What kind of physical mechanisms that actually govern dynamic wetting phenomena have been a matter of controversy and argument in the recent literature (Blake & Shikhmurzaev 2002; Eggers & Evans 2004; Shikhmurzaev & Blake 2004), where these viewpoints have been based on different theoretical approaches (Blake 2006; Bonn *et al.* 2009). Even though extensive research has been directed towards wetting physics, many phenomena with moving contact lines are still not well understood. An example of such is the understanding of the physical processes that govern rapid dynamic wetting, which still holds challenges.

Despite the apparent simplicity of placing a small water droplet on a glass plate, the prediction of its evolution after contact with the solid surface is non-trivial. A number of physical phenomena in the bulk and at the solid surface influence the evolution of the spreading droplet. This is particularly true during the initial phase of wetting, when the contact line speed is typically the greatest. In this case, experimental investigations show (Biance, Clanet & Quere 2004; Drelich & Chibowska 2005; Bird, Mandre & Stone 2008) that the initial speed of the contact line of water on a hydrophilic surface is of the order of metres per second.

† Email address for correspondence: andreaca@mech.kth.se
‡ Present address: Osquars Backe 18, SE-100 44 Stockholm, Sweden.

https://doi.org/10.1017/jfm.2011.211 Published online by Cambridge University Press

General reviews of wetting phenomena are given by de Gennes (1985), Blake (2006) and Bonn *et al.* (2009). In the following, we will discuss literature particularly relevant for the very rapid wetting processes that are the subject of this paper.

The contact line is formed as the interface between a gas and a liquid, or two immiscible liquids, interacts with a solid substrate. A classical problem in fluid dynamics has been that the Stokes equations allow a solution for the flow in the vicinity of the contact line, which, however, exhibits a non-integrable singularity of the viscous stress at the wall (Huh & Scriven 1971). This singularity can be removed formally if the no-slip condition at the wall is relaxed. The root of the problem is, however, that the continuum description breaks down and that phenomena at molecular length scales must somehow be accounted for. Allowing slip on the wall and using Navier–Stokes equations, Voinov (1976) and Tanner (1979) derived a relationship between the apparent or observable contact angle and the capillary number (Ca) (Blake 2006)

$$\theta_D^3 - \theta_m^3 = 9Ca\ \ln\left(\frac{h}{h_m}\right). \tag{1.1}$$

Here, θ_D is the apparent contact angle, i.e. the angle between the macroscpically observable interface and the solid wall, θ_m is the microscopic contact angle at the solid surface, which is usually assumed to be the equilibrium contact angle, Ca is the Capillary number, $Ca = \mu U/\sigma$, giving the ratio between the viscous and surface tension force, μ is the droplet viscosity, U the wetting speed and σ is the surface tension coefficient.

The equation is derived based on the assumption that $\theta_D < 3/4\pi$ and that the characteristic length h, e.g. droplet diameter, is much larger than the microscopic length h_m, $h \gg h_m$. The singularity at the solid surface is circumvented here by introducing the slip-length, an ad-hoc length of microscopic size h_m. It is commonly determined (h_m) by curve fitting of the equation to experimental results. A similar result to Voinov (1976) and Tanner (1979) was obtained by Cox (1986), based on an asymptotic reduction of the Navier–Stokes equations. These results generally match available experimental data well, such as the experiments from Hoffman (1975). In the hydrodynamic theory, the surface tension force generated by the local curvature near the contact line is believed to be the driving mechanics behind contact line motion, whereas viscosity in the bulk is resisting its motion.

Another physical explanation of contact line motion was proposed by Blake & Haynes (1969), a theory that is often referred to as the molecular kinetics (MK) theory. Contact line movement is considered here to be an active process at the molecular adsorption sites on the solid surface. The molecules are assumed to hop back and forth between adsorption sites with a characteristic frequency (k_0), where they move over a molecular distance (λ). Based on Eyring's theory of absolute reaction rates (Glasstone, Laidler & Eyring 1941), the frequency of molecular transfer due to the forward (K^+) and backward (K^-) hopping can be expressed as (Ren & E 2007)

$$K^+ = k_0 \exp\left(\frac{w}{2nk_bT}\right), \quad K^- = k_0 \exp\left(\frac{-w}{2nk_bT}\right), \tag{1.2}$$

where n is the number of adsorption sites per unit area, k_b the Boltzmann constant and T the temperature. $w = \sigma(\cos(\theta_0) - \cos(\theta))$ is the work done due to the uncompensated Young's stress by having a non-equilibrium contact angle, where θ_0 is the equilibrium contact angle and θ is the dynamic contact angle. This gives the relationship for the

https://doi.org/10.1017/jfm.2011.211 Published online by Cambridge University Press

velocity of the moving contact line as

$$V_{MK} = \lambda(K^+ - K^-) = 2k_0\lambda \sinh\left(\frac{\sigma(\cos(\theta_0) - \cos(\theta))}{2nk_bT}\right). \tag{1.3}$$

At equilibrium, backward and forward hopping are equal as are the dynamic and equilibrium contact angles, predicting no contact line motion.

Despite the fact that these two theories are formulated on different length scales and from very different points of view, they have both been applied with success. This suggests that the hydrodynamic and molecular kinetic theory each captures different wetting physics. It should be noted that no active molecular processes are accounted for in the hydrodynamic theory and that the MK theory does not include any influence from viscosity. A combined model was proposed by Petrov & Petrov (1992) that merges these two approaches, in an attempt to capture a broader spectrum of wetting phenomena.

Experimental investigations of droplet spreading have historically been mainly focused on the rather slow viscously dominated spreading regime, such as the work by Hoffman (1975) and Ngan, Dussan, & Elizabeth (1982) to name a few. These experiments have been well explained by already existing theoretical models, such as the one by Voinov–Tanner. Experiments have earlier been limited in both temporal and spatial resolution, making certain rapid wetting phenomena inaccessible. An example of such is the short-time spreading of a water droplet on a glass surface. The advent of high-speed cameras has now made such wetting phenomena experimentally accessible, and in recent years experimental results have appeared (Biance *et al.* 2004; Saiz & Tomsia 2004; Drelich & Chibowska 2005; Bird *et al.* 2008). The observations have many similarities, such as the temporal evolution of the droplet shape, where the observable contact angle highly differs from the equilibrium value as the droplets spread. In these rapid spreading experiments, the contact line moves with a characteristic velocity of the order of metres per second.

Bird *et al.* (2008) captured in detail, with a high-speed camera (67 000 frames s^{-1}), the temporal contact line evolution for droplets spreading on solid surfaces with varying wettability. In these experiments, also the initial rapid wetting phase was captured. By varying the droplet size, viscosity and surface wettability, they showed that the time scale for the phenomena failed to follow a viscous scaling. A striking finding was made, as the experiments fell on a master curve based on an inertial time scale. This indicates that inertia might resist wetting. They also found that the slope of the spreading rate depended on the equilibrium contact angle of the surface. Additional spreading data were provided in Courbin, Bird & Stone (2009), in an attempt to expand the collapse with a viscous scaling. It was also shown that the spreading power law response depended on the initial shape of the droplets.

Ren & E (2007) identified a similar rapid wetting regime, at the nano-scale, in molecular dynamics simulation. They described this flow regime as the onset of non-linearity, due to the large local forcing acting in the contact line region. This flow was suggested to be an active or diffusive process, at the contact line. It was pointed out that this type of wetting physics still remains unclear, and further investigations are needed to identify the governing wetting mechanisms.

An alternative way of obtaining models of wetting phenomena is through the use of phase field theory, which is based on a phenomenological description of the free energy of the system. The phase field framework enables contact line motion due to diffusive interfacial fluxes, in other words, a different mechanism from those mentioned above. For relatively slow wetting phenomena, situated in the same wetting regime

https://doi.org/10.1017/jfm.2011.211 Published online by Cambridge University Press

as Voinov–Tanners theory and Hoffmann's experiments, the phase field theory has proven both analytically (Jacqmin 2000) as well as numerically (Briant & Yeomans 2004; Villanueva & Amberg 2006; Yue, Zhou & Feng 2010) to capture such wetting physics. Briant & Yeomans (2004) found the contact line diffusion to vary over a length scale different from the interface width, and by scaling arguments showed that this length is related to the mobility constant multiplying the chemical potential. Yue *et al.* (2010) made a modification to the scaling of the diffusion length and interpreted the microscopic length in Voinov–Tanners theory (h_m) in terms of the contact line diffusion length from the phase field theory. It should be noted that all of these results are obtained by making the physical assumption that the interface is close to an equilibrium state as it wets the solid.

The equilibrium boundary condition, mentioned above, has been expanded to a general boundary condition by Qian, Wang & Sheng (2006*a*), which has been explained by Onsager's principles of minimum dissipation (Qian, Wang & Sheng 2006*b*). By extracting the phase field parameters and local slip at the surface from molecular dynamics simulations, used as input parameters in the phase field model, a direct match of the interface and slip profile could be obtained at the nano-scale (see Qian *et al.* 2006*b*; Qian, Wang & Sheng 2004). An important point, is that these simulations fall in the same category as the results from Villanueva & Amberg (2006) and Yue *et al.* (2010) as they are in this context considered to have rather slow wetting dynamics.

In our recent paper (Carlson, Do-Quang & Amberg 2009), we showed that the assumption of local equilibrium at the solid surface is deficient in the rapid dynamic wetting regime, and that the phase field, or diffuse interface, framework, provides a rather natural way to incorporate non-equilibrium effects at the contact line. This implies that there is an important relaxation process from a non-equilibrium towards an equilibrium state. Within the phase field framework, the boundary condition that accounts for such wetting physics, follows directly from the variational formulation of the free energy in the system (see Jacqmin 2000). We showed (Carlson *et al.* 2009) that by including the effects of non-equilibrium in the boundary condition at the solid surface, a direct match could be obtained with the detailed experimental results by Bird *et al.* (2008). In the contact line formulation at the solid surface, a rate coefficient D_W appears, which was interpreted in terms of parameters from the MK theory. Jacqmin (2000) was to our knowledge the first to discuss this boundary condition and he made a rough estimate of the magnitude of D_W, based on molecular dynamics simulation data from Matsumoto, Maruyama & Saruwatari (1995). The magnitudes of the coefficients found by Carlson *et al.* (2009) and Jacqmin (2000) are in reasonable agreement. Thus, it is believed that this general wetting formulation encompasses wetting regimes that have previously been captured with the hydrodynamic and the MK theory.

Four different regimes have been presented in the literature, which are said to describe the force balances and dissipation mechanisms in dynamic wetting, at different stages. These are the initial cusp, inertia and viscous wetting from the hydrodynamic theory and molecular contact line friction from the molecular kinetic theory. In the very first short-time spreading, the interface forms a small cusp region where viscosity is believed to dominate the spreading dynamics (Eggers, Lister & Stone 1999; Biance *et al.* 2004). This initial spreading regime takes place as the droplet starts to spread onto the solid, where a small region with a high curvature drives the flow. As the length scales are small, the flow has a low Reynolds number (Re), describing the relative importance between inertia and viscous forces,

https://doi.org/10.1017/jfm.2011.211 Published online by Cambridge University Press

and viscosity is impeding the contact line motion that is driven by interfacial energy.

As the contact line propagates across the solid surface, the spreading radius increases and the liquid in the bulk of the droplet is accelerated, consequently increasing the inertial forces in the flow. When sufficient bulk liquid is accelerated, inertia is dominating over the initial viscous dissipation and constitutes the main hindrance for droplet spreading. The inertial spreading was found to obey the laws predicted by Eggers *et al.* (1999), also found experimentally by Aarts *et al.* (2005). By following the same reasoning as Eggers, Biance *et al.* (2004) and Aarts *et al.* (2005) found the spreading radius for inertial wetting to also scale with the square root of time. Geometrical arguments about the flow, forced by symmetry in the direction perpendicular to contact and that both seemingly are driven by gradients in curvature provides an analogy between droplet coalescence and spreading. Nonetheless, droplet spreading cannot be fully explained by gradients in curvature since the solid's equilibrium contact angle is experimentally found to influence the power-law response to the spreading curve (Bird *et al.* 2008).

In the late time dynamics, the droplet has a slow, nearly steady motion as it relaxes towards its equilibrium contact angle. This slow wetting dynamics is often characterized by the capillary number Ca, and viscous dissipation in the whole bulk is the main source for the resistance to contact line motion. The slow viscously dominated wetting has been well defined by classical wetting relations as derived by Voinov (1976), Tanner (1979) and Cox (1986). By assuming that the droplet has a spherical cap and applying Tanners law (Biance *et al.* 2004), the relationship between the spreading radius (r) and time (t) can be derived, and scales with $r \sim t^{1/10}$. The expressions for the inertial and viscous spreading radii then yield a criterion for the transition between inertial and viscous wetting, as described by Biance *et al.* (2004).

The molecular kinetic theory describes a different dissipative mechanism than what is predicted with the hydrodynamic theory. Here, the dissipation arises from the advancing contact line region due to the attachment of liquid molecules at the solid surface (De Coninck, de Ruijter & Voue 2001). The spreading radius in this regime is found to scale with $r \sim t^{1/7}$ and has been identified at later time scales, taking place after the inertial spreading regime described above (De Coninck *et al.* 2001; Seveno *et al.* 2009).

Recent experimental findings suggest that at even shorter time spreading none of the regimes discussed above are appropriate, one indication being that the equilibrium contact angle seems to be a less important parameter here (Bird *et al.* 2008). Two questions that remain are; if there exist additional dissipative mechanisms that might influence the spreading dynamics at very short times; and at what time scales do they govern the contact line motion?

The main purpose of this paper is to present a mathematical model of very rapid spreading and, guided by results from this, elucidate the physics governing a rapid dynamic wetting process. In the next section, the mathematical model is motivated and presented, including a new rate coefficient (D_W), which we will argue captures molecular interactions at the contact line. In § 3, we present detailed simulations of recent experiments on rapidly spreading droplets. In § 4, we wish to identify the primary cause for resistance to spreading, by computing the evolution of the kinetic energy in the flow, as well as dissipation due to viscous stresses, and molecular processes at the contact line, etc. The relative magnitude of these is studied as the droplet evolves. We finally make some concluding remarks.

https://doi.org/10.1017/jfm.2011.211 Published online by Cambridge University Press

2. Phase field theory

The phase field, or diffuse interface, model is formulated here for a binary mixture of two immiscible fluids (gas or liquid), and includes the surface energies of fluid–fluid and fluid–solid interfaces. The formulation starts from a postulated free energy F of the system, as a functional of the fluid mixture composition C

$$F = \int_{\Omega} \left(\beta \Psi(C) + \frac{\alpha}{2} |\nabla C|^2 \right) \mathrm{d}\Omega + \int_{\Gamma} (g(C)(\sigma_{sg} - \sigma_{sl}) + \sigma_{sl}) \, \mathrm{d}\Gamma. \tag{2.1}$$

The free energy has one contribution from the bulk (Ω) and one from the bounding solid surfaces (Γ). The first term in the integral over the volume Ω is the bulk potential, which is chosen here in the conventional way as $\Psi = (1/4)(C+1)^2(C-1)^2$. This function has two local minima which implies that the only stable equilibrium values that C can take are $+1$ or -1. These values thus denote regions occupied by one of the two pure fluids in the mixture. In what follows, we will consider water and air, with $C = 1$ for water and $C = -1$ for air. The second term in the bulk integral introduces the surface energy of fluid–fluid interfaces. The competition between the bulk and interfacial energy forms an interface, separating the two phases. β and α are phase field parameters, originating from the multi-variable Taylor expansion about the free energy per molecule (see Cahn & Hilliard 1958). These determine the surface energy σ and the width of fluid–fluid interfaces ϵ according to $\beta = 3\sigma/2\sqrt{2}\epsilon$ and $\alpha = \sigma\epsilon(3/2\sqrt{2})$, or conversely $\sigma = (2\sqrt{2}/3)\sqrt{\alpha\beta}$ and $\epsilon = \sqrt{\alpha/\beta}$.

The free energy at the solid surface (Jacqmin 1999), is formulated as an integral over the solid boundary Γ of the local surface energy. The function $g(C) = 0.5 - 0.75C + 0.25C^3$ is a smoothly varying function which is equal to 0 for a wet wall (C = 1) and 1 for a dry wall (C = −1). It thus acts as a switch that changes the surface energy between σ_{sg} for a dry and σ_{sl} for a wet solid surface. The choice of the function $g(C)$ is made so that, together with the choice of the double well function $\Psi(C)$, it will give an equilibrium contact angle consistent with Young's law.

By taking the variational derivative of the free energy (F) with respect to the order parameter C and integrating by parts, we obtain

$$\delta F = \int (\beta \Psi'(C) - \alpha \nabla^2 C) \delta C \, \mathrm{d}\Omega + \int (\alpha \nabla C \cdot \boldsymbol{n} + g'(C)[\sigma_{sg} - \sigma_{sl}]) \delta C \, \mathrm{d}\Gamma. \tag{2.2}$$

The integrand of the volume integral defines the bulk chemical potential $\phi^* = \beta\Psi'(C) - \alpha\nabla^2 C$. The surface integral defines the boundary condition for the chemical potential, accounting for the variation in free energy at the surface. The surface integral represents the wetting boundary condition where $\boldsymbol{n}$ is the surface normal. This boundary condition will be analysed further below. By minimizing both the bulk contribution of the chemical potential with respect to the order parameter C, the equilibrium profile for a flat interface can be obtained as $C_0(x) = \tanh(1/\sqrt{2}\epsilon x)$. The expression for surface energy $\sigma = (2\sqrt{2}/3)\sqrt{\alpha\beta}$ is readily obtained by inserting the equilibrium profile for C in the expression for free energy (2.1) and integrating over the interface.

Van der Waals was the first to propose a free energy formulation similar to the one given above, where a diffuse interface separates the two different fluids. Cahn & Hilliard (1958) extended Van der Waals theory to a time-dependent situation by approximating the diffusive fluxes as proportional to gradients of the chemical potential,

$$\frac{\partial C}{\partial t} + \boldsymbol{u}^* \cdot \nabla C = -\nabla \cdot \boldsymbol{J} = \nabla \cdot (M \nabla (\beta \Psi'(C) - \alpha \nabla^2 C)), \tag{2.3}$$

https://doi.org/10.1017/jfm.2011.211 Published online by Cambridge University Press

where $-\boldsymbol{J} = M\nabla\phi^*$ is a flux. We have here also accounted for the effects of the fluid motion and M is a mobility that is considered to be constant.

2.1. *Equilibrium wetting boundary condition*

Within the phase field theory, the boundary condition that accounts for the free energy distribution between the different phases, sets the wetting boundary condition for the interface (see (2.2)). By making the assumption that the interface is at local equilibrium as it wets the solid surface, the boundary condition becomes (Villanueva & Amberg 2006)

$$\alpha\nabla C\cdot\boldsymbol{n} + \sigma\cos(\theta_0)g'(C) = 0. \tag{2.4}$$

We have used the Young's equation relating the equilibrium static contact angle to the surface tension coefficients (σ): $\sigma\cos(\theta_0) = \sigma_{sg} - \sigma_{sl}$.

The assumption of local equilibrium at the solid surface has been a widespread assumption in phase field wetting simulations, which has proven to be successful in describing numerous physical phenomena involving moving contact lines (Jacqmin 1999; Villanueva & Amberg 2006; Ding & Spelt 2007; Do-Quang & Amberg 2009; Yue *et al.* 2010). One of the strong arguments that speak in favour of the equilibrium assumption is that it has been found in good agreement with the hydrodynamic wetting theory. Yue *et al.* (2010) matched phase field simulations with the wetting relation by Cox (1986) and proposed a new interpretation of the *ad hoc* microscopic length needed in this relation. This length was found to scale with the mobility between the phases and the viscosity. Villanueva & Amberg (2006) showed that numerical phase field wetting simulations were in good agreement with the experimental results of Hoffman (1975). Hoffmann's experiments show a fairly universal relationship between the apparent, observable, contact angle and the capillary number. This is in good agreement with the analytical expressions by Voinov (1976), Tanner (1979) and Cox (1986). Based on the equilibrium wetting condition, Jacqmin (1999) showed using asymptotic analysis that the phase field boundary condition given in (2.4) converged to a relationship between the apparent contact angle and the capillary number.

2.2. *Non-equilibrium wetting boundary condition*

Although the equilibrium wetting assumption has been found to capture many physical wetting phenomena, it has been demonstrated by Carlson *et al.* (2009) that this assumption is inadequate for rapidly spreading droplets. In order to capture this rapid wetting regime, which has an additional dissipative mechanism, it is crucial to allow for a relaxation from non-equilibrium towards an equilibrium state. A non-equilibrium boundary condition is incorporated in the phase field framework, and has been discussed previously by different authors (see Jacqmin 2000; Qian, Wang & Sheng 2003). However, its importance in practical simulations has only just recently been investigated (Carlson *et al.* 2009).

The boundary condition in (2.4) is modified to account for non-equilibrium at the contact line. The phenomenological argument inherent in the phase field method, leading from a free energy to partial differential equations, consists of requiring the irreversible evolution of the system to be such that the free energy is always decreasing. The boundary condition as given in (2.4) will not give any dissipation at the contact line. This is readily modified to allow for dissipation, if, instead of setting the argument of the surface integral in (2.2) to zero, permissible changes in C are made proportional to $\alpha\nabla C\cdot\boldsymbol{n} + \sigma\cos(\theta_0)g'(C)$, so that the resulting change in free energy is negative definite. The off-equilibrium perturbations are counteracted by a diffusive flux proportional to $D_W^*(\partial C/\partial t)$, where D_W^* is a phenomenological parameter,

https://doi.org/10.1017/jfm.2011.211 Published online by Cambridge University Press

analogous to a mobility, leading to a non-zero contribution on the right-hand side of (2.4). This gives then the non-equilibrium boundary condition governing rapid wetting

$$\alpha \nabla C \cdot \boldsymbol{n} + \sigma \cos(\theta_0) g'(C) = D_W^* \frac{\partial C}{\partial t}. \tag{2.5}$$

Here, D_W^* is believed to originate from the molecular interactions at the contact line, as they reorganize in a diffusive process causing contact line motion (Carlson *et al.* 2009). No-slip is prescribed at the solid surface.

2.3. *Governing equations for the fluid motion*

We consider here a system consisting of a two-phase flow of air and water, where both are considered as incompressible. Experiments have shown (Bird *et al.* 2008) that the contact line has a maximum speed of around 1 m per second, so no significant compressible effect is expected in the air and it is therefore treated here as an incompressible phase

$$\nabla \cdot \boldsymbol{u}^* = 0, \tag{2.6}$$

$$\rho^*(C)\left(\frac{\partial \boldsymbol{u}^*}{\partial t} + (\boldsymbol{u}^* \cdot \nabla)\boldsymbol{u}^*\right) = -\nabla P^* + \nabla \cdot (\mu^*(C)(\nabla \boldsymbol{u}^* + (\nabla \boldsymbol{u}^*)^{\mathrm{T}})) - \rho(C) g \boldsymbol{e}_z - C \nabla \phi^*, \tag{2.7}$$

where $\boldsymbol{u}^*$ is the velocity and P^* is the modified pressure (see Jacqmin 1999). $\rho(C)$ and $\mu(C)$ are the fluid density and dynamic viscosity, which are given as functions of the order parameter C; $\rho^*(C) = (1/2)(\rho_l(C+1) - \rho_g(C-1))$, $\mu^*(C) = (1/2)(\mu_l(C+1) - \mu_g(C-1))$. The subscript l denotes liquid and the subscript g denotes gas, using the material parameters for water and air, g is gravity and $\boldsymbol{e}_z$ is the unity vector in the z-direction. The last term is expressing the potential form of the surface tension force, proposed by Jacqmin (1999).

2.4. *Non-dimensional formulation*

The governing equations are made dimensionless based on the characteristic parameters of the flow, giving the dimensionless variables

$$z^* = Lz, \quad t^* = \frac{L}{U}t, \quad P^* = \frac{\mu_l U}{L}P, \quad u = Uu^*, \quad \phi^* = \frac{3\sigma}{2\sqrt{2}\epsilon}\phi, \tag{2.8}$$

where the dimensional variables are denoted with *. L is a characteristic length scale, here chosen as the initial droplet radius, and U is the reference velocity. The reference velocity is considered to be the capillary speed $U = \sigma/\mu$. By introducing this scaling into the Navier–Stokes and the Cahn–Hilliard equation we obtain their non-dimensional form, here considered in cylindrical coordinates

$$\nabla \cdot \boldsymbol{u} = 0, \tag{2.9}$$

$$\frac{\partial C}{\partial t} + \boldsymbol{u} \cdot \nabla C = \frac{1}{Pe}\nabla^2 \phi = \frac{1}{Pe}\nabla^2(\Psi'(C) - {C_n}^2 \nabla^2 C), \tag{2.10}$$

$$\frac{\rho(C)}{\rho_l}\left(\frac{\partial \boldsymbol{u}}{\partial t} + (\boldsymbol{u} \cdot \nabla)\boldsymbol{u}\right) = -\nabla P + \frac{1}{Re}\left(\nabla \cdot \left(\frac{\mu(C)}{\mu_l}(\nabla \boldsymbol{u} + (\nabla \boldsymbol{u})^{\mathrm{T}})\right) - \frac{Bo}{Ca}\frac{\rho(C)}{\rho_l}\boldsymbol{e}_z - \frac{C \nabla \phi}{C_n \cdot Ca}\right). \tag{2.11}$$

This gives five non-dimensional numbers

$$Pe = \frac{2\sqrt{2}U\epsilon L}{3M\sigma}, \quad C_n = \frac{\epsilon}{L}, \quad Re = \frac{\rho_l U L}{\mu_l}, \quad Ca = \frac{2\sqrt{2}\mu_l U}{3\sigma}, \quad Bo = \frac{(\rho_l - \rho_g)gL^2}{\sigma}. \tag{2.12}$$

https://doi.org/10.1017/jfm.2011.211 Published online by Cambridge University Press

The Peclet number (Pe) expresses the ratio between the advection and diffusion. The Cahn number (C_n) expresses the ratio between the interface width and the characteristic length scale. The Reynolds number (Re) expresses the ratio between the inertia and viscous forces. The Capillary number (Ca) expresses the ratio between the viscous and the surface tension force. The Bond number (Bo) expresses the ratio between the gravitational and surface tension force.

The wetting boundary condition is scaled in accordance with Carlson *et al.* (2009) $D_W^* = (k_B T)/(\lambda^2 k_0)$, where λ is the molecular hopping length, k_0 their characteristic frequency, k_b is the Boltzmann constant and T the temperature. This gives the dimensionless general wetting boundary condition

$$D_W \frac{\partial C}{\partial t} = C_n \nabla C \cdot \boldsymbol{n} + \cos(\theta_0) g'(C). \tag{2.13}$$

Here, $D_W = D_W^*/(\mu L) = Kn\,/Ag$ is a phenomenological parameter and described in terms of two additional non-dimensional numbers, where $Kn = \lambda/L$ is a type of Knudsen number giving the ratio between the molecular hopping length and the characteristic length scale. In the phase field context, it is natural to interpret Kn in terms of the Cahn number, which we will return to below. $Ag = \mu_l/(U_M \sigma_M)$ is a new non-dimensional number, where $U_M = k_0 \lambda$ is the mean molecular hopping velocity and $\sigma_M = (k_b T)/\lambda^2$ is the energy required to break the liquid–solid bonds due to the hopping between adsorption sites. Thus, Ag represents the ratio between the viscous force and the energy needed to break solid–liquid bonds associated with molecular hopping (Carlson *et al.* 2009).

On all solid walls a no-slip boundary condition $\boldsymbol{u} = 0$ is imposed, and a Neumann boundary condition is applied for the pressure. *Vice versa* apply for the outlets of the domain, with a Neumann boundary condition for the velocities, and the pressure is defined as $P = 0$.

2.5. *Computational methodology*

The axi-symmetric governing equations have been solved numerically with the finite-element toolbox FemLego (Amberg, Tonhardt & Winkler 1999). FemLego is an open-source symbolic tool for solving partial differential equations. Within a single Maple worksheet, the partial differential equations, boundary conditions and numerical solvers are all defined. It inherits parallel computational and adaptive mesh refinement capabilities (see Do-Quang *et al.* 2007 for details).

The Cahn–Hilliard equation has been solved with a type of precondition conjugate gradient (CG) solver, described by Villanueva & Amberg (2006). The multifluid Navier–Stokes equations have been solved with a projection scheme, which was proposed by Guermond & Quartapelle (2000). The linear system for the velocities and pressure have been, respectively, solved with the general minimum residual method and a CG solver. All variables are approximated with linear base functions and the mesh consists of triangular elements.

An adaptive mesh refinement method has been applied in the simulations (Do-Quang *et al.* 2007), enabling a high resolution of the key features in the flow, here being the interface. This allows us to resolve small length scales in the flow without having an excessive computational time. The droplet radius is discretized with approximately 40 node points and the interfacial area has about a six times higher mesh resolution.

https://doi.org/10.1017/jfm.2011.211 Published online by Cambridge University Press

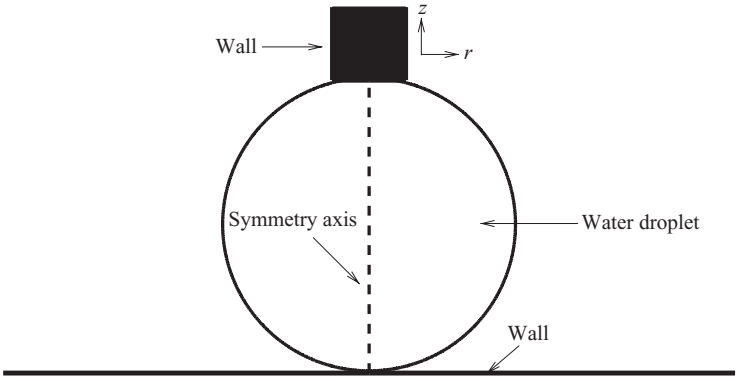


FIGURE 1. Simulation setup and the initial condition.

3. Prediction of spontaneous spreading of water droplets

3.1. *Scope and simulation set-up*

Here, we will present numerical simulations in direct accordance with the droplet spreading experiments performed by Bird *et al.* (2008). A water droplet with a radius $L = 0.78$ mm in air is simulated as it wets three solid surfaces with different degrees of wettability. The material properties for air are denoted by the subscript g and the material properties for water are denoted by the subscript l. The density is $\rho_l = 998\,\mathrm{kg\,m^{-3}}$, $\rho_g = 1.2\,\mathrm{kg\,m^{-3}}$, the viscosity is $\mu_l = 10^{-3}\,\mathrm{Pa\,s}$, $\mu_g = 1.6 \times 10^{-5}\,\mathrm{Pa\,s}$, gravity is $g = 9.81\,\mathrm{m\,s^{-2}}$ and the surface tension coefficient is $\sigma = 0.073\,\mathrm{N\,m^{-1}}$. This gives the characteristic capillary velocity $U = \sigma/\mu_l = 73\,\mathrm{m\,s^{-1}}$; it should, however, be noted that the actual speed in the simulations is much less than this value $U_{max} \sim 1\,\mathrm{m\,s^{-1}}$. This gives then the non-dimensional numbers based on the liquid material properties, $Re = 56\,940$, $Ca = 1$ and $Bo = 0.08$. The mass diffusion coefficient has been chosen as $D = 5.7 \times 10^{-6}\ \mathrm{m^2\ s^{-1}}$ giving a Peclet number $Pe = 1 \times 10^4$. The choice of Pe for the simulations presented here does not influence the results. A short discussion around the influence of Pe on the flow is presented below. In addition to the material properties for the gas and liquid, we define the static equilibrium contact angle for the three solid surfaces as $\theta_0 = [3^\circ, 43^\circ, 117^\circ]$. Since these parameters are the same as in the experiments by Bird *et al.* (2008), we choose to keep these fixed in the simulations, where we only vary the rate coefficient D_W that is determined from the experimental data. After determining D_W, the model has, in principle, no adjustable parameters, as we will show below that the width of the interface does not influence the simulation results in a noticeable way. The model as presented enables then modelling of dynamic wetting without making any *ad hoc* physical assumptions.

Figure 1 shows the axi-symmetric simulation set-up and the initial condition. Initially, the droplet has a spherical shape and is placed underneath a rod, imitating the needle used in the experiments. In the simulations, the contact line is allowed to move across the surface of the rod, while in the experiments liquid is always retained at the tip of the needle. In order to keep the droplet attached to the rod surface, it has been given an equilibrium contact angle of $\theta_0 = 90^\circ$. At the lower surface, which the droplet spreads onto, the non-equilibrium boundary condition 2.5 is used. In order to minimize the influence of the initial condition in the simulations, the droplet is at first not put in direct contact with the wall. It is placed so that a thin air layer, in the wall-normal direction, separates the interface and the wall with a thickness that

https://doi.org/10.1017/jfm.2011.211 Published online by Cambridge University Press

is less than the interface width. This way the onset of wetting is captured without initially prescribing an artificial contact angle at the surface.

3.2. *Spreading rate*

The detailed evolution of the contact line motion of droplets spreading over solid surfaces with different degrees of wettability was described by Bird *et al.* (2008). Their experiments provide excellent data for a fidelity check of macroscopic contact line models for dynamic wetting, as the observed contact angle, in these experiments, changes in time as the droplets spread. We have here extracted and focused on the experimental results of water droplets with a radius $L = 0.78$ mm, that wets three solid surfaces with different degrees of wettability $\theta_0 = [3^\circ, 43^\circ, 117^\circ]$.

Figure 2 shows the sensitivity and influence of the parameter D_W on the spreading rate as the water droplets wet the different surfaces. Figure 2(*a*) shows the temporal evolution of the contact line as the droplet spreads over a surface with an equilibrium angle $\theta_0 = 3^\circ$. One clear observation is that the equilibrium assumption ($D_W = 0$) is deficient, as the contact line propagates too fast over the surface. By increasing the coefficient D_W, dissipation is added at the contact line, resulting in a deceleration of the relaxation process towards thermodynamic equilibrium. Best fit with the experimental result is found for $D_W = 1.0$.

For wetting on a solid surface with an equilibrium contact angle $\theta_0 = 43^\circ$ (see figure 2*b*), a similar overall picture as in figure 2(*a*) is observed. The assumption of local equilibrium at the contact line, makes it propagate too fast in comparison with the experimental result by Bird *et al.* (2008). The best match with the experimental results was found for $D_W = 1.4$. We notice that the speed of the contact line is lower here ($\theta_0 = 43^\circ$) than what was observed on a surface that is more wettable (see figure 2*a*). This effect is due to a lower local forcing in the contact line region, as the initial wetting is closer to its equilibrium state.

For a nearly hydrophobic surface ($\theta_0 = 117^\circ$), the equilibrium assumption seems to give results that are quite coherent with the experimental wetting (see figure 2*c*). A slight improvement might be seen in the spreading prediction using the coefficient, $D_W = 0.2$.

To summarize the results in figure 2, we notice that, for the case studied here, the equilibrium wetting boundary condition fails to correctly predict the wetting speed on hydrophilic surfaces. By introducing another dissipative mechanism, we thus obtain a direct agreement with the experimental results by Bird *et al.* (2008). The rate coefficient appearing in the non-equilibrium boundary condition is determined from the experimental data, and best fit is observed for $D_W = [1.0, 1.4, 0.2]$ for surfaces with $\theta_0 = [3^\circ, 43^\circ, 117^\circ]$, and have been condensed into *figure 1* in Carlson *et al.* (2009). D_W is believed to be a physically reasonable parameter that should naturally vary for different systems. We are at the present time lacking a rational explanation for the non-monotonic behaviour of the coefficient D_W for the different contact angles, investigated here. However, it should be noted that ongoing work based on a micro-scale analysis is in progress, but beyond the scope of the present paper.

One peculiar feature that was identified by Bird *et al.* (2008) was that, by using an inertial time scale, the experimental spreading results fell on a master curve, irrespective of droplet size. The spreading curve was found to follow a power law, but the exponent found in the experiments changed with the wettability of the solid substrate. The data did not collapse when a more intuitive viscous time scaling was used. In figure 3, droplet radius is plotted versus time in logarithmic units, where the triangles are intended to more clearly illustrate the different exponents observed

https://doi.org/10.1017/jfm.2011.211 Published online by Cambridge University Press

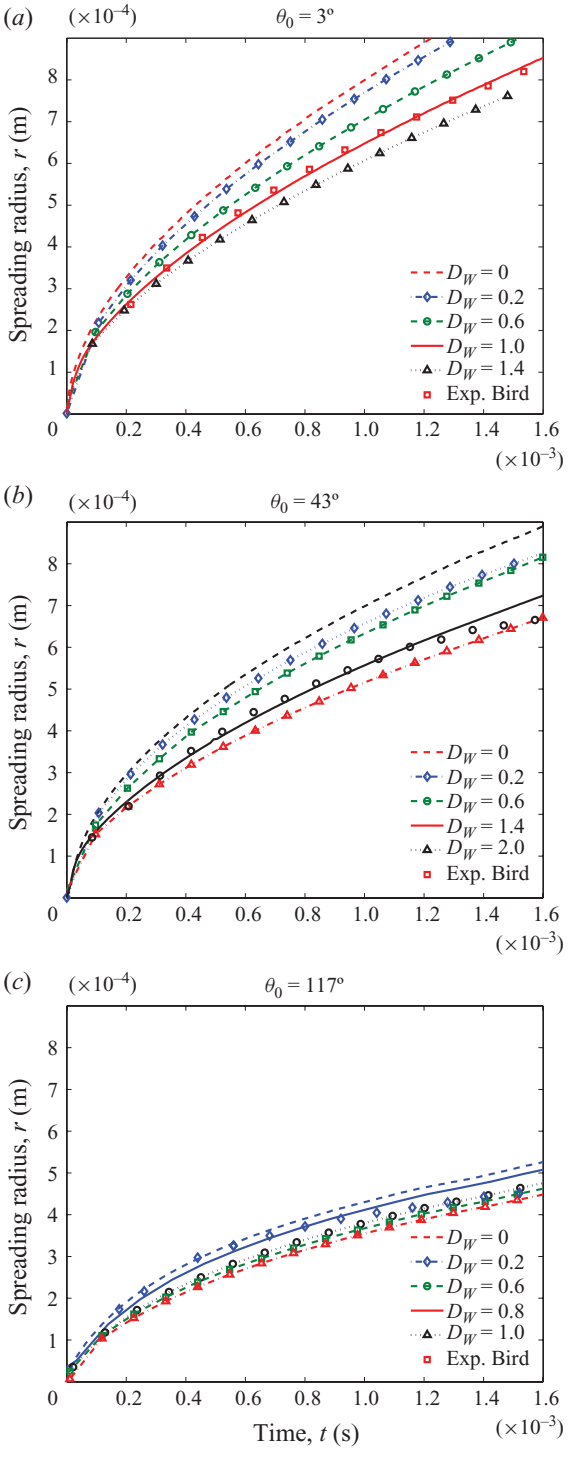


FIGURE 2. (Colour online available at journals.cambridge.org/FLM) The temporal evolution droplets spreading radius with $L = 0.78$ mm and the influence of D_W on the results as it wets three solid surfaces with different degrees of wettability; $\theta_0 = [3°, 43°, 117°]$. The fully drawn line, in each sub-figure, represents the best match with the experiment.

https://doi.org/10.1017/jfm.2011.211 Published online by Cambridge University Press

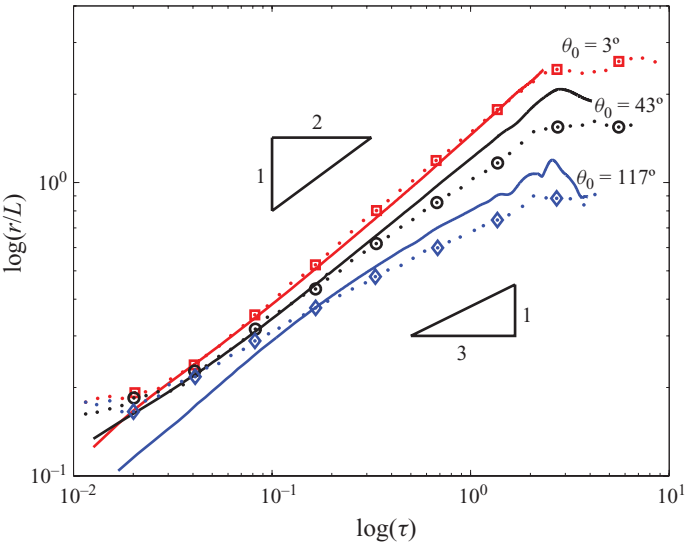


FIGURE 3. (Colour online) Comparison between the experimental and numerically predicted droplet spreading radius with logarithmic axes. The full lines denote the simulations and the dotted lines with markers the experimental master curve from Bird *et al.* (2008).

in the power-law for the different solid substrates. Here, a non-dimensional time $\tau = t/(\sqrt{(\rho_l L^3)/\sigma})$ is used, to facilitate comparison with Bird *et al.* (2008). It should be noted that Bird *et al.* (2008) points out that less emphasis should be placed on their results for the initial wetting ($\tau = t/(\sqrt{(\rho R^3)/\sigma}) < 0.1$), due to the spatial accuracy of their measurements.

The slight discrepancy at late times is likely an effect of differences in the experimental and computational set-up. At late times in the experiments, the droplet starts to detach from the needle by forming a thin liquid neck that finally pinches off, where liquid is always retained at the tip of the needle. In the simulations, a rod mimics the needle, allowing the contact line to move. This would influence the size of the smaller secondary droplet as well as the time for the collapse of the liquid neck as the larger droplet detaches.

A dramatic change in the spreading characteristics is observed for all three cases around the time $\tau = 3$ in both the simulations and the experiments. The same behaviour was found also with the equilibrium boundary condition. This spreading behaviour was explained as a transition between the inertial and the viscously dominated wetting (Bird *et al.* 2008). The simulations of a highly wettable surface ($\theta_0 = 3°$) are stopped before this time, since the contact line leaves the domain before reaching the transition. Later, in this article, we will present the dissipative mechanisms and the rate-of-change of kinetic energy.

By applying the criterion for the transition between inertial and viscous wetting, proposed by Biance *et al.* (2004), we obtain a specific time $\tau_t \sim ((\rho\sigma L)/\mu^2)^{1/8}$, when the transition should approximately take place. By introducing the material parameters for the simulated cases, we obtain $\tau = 3.9$, which is in good agreement with the experimental and numerical data (see figure 3).

https://doi.org/10.1017/jfm.2011.211 Published online by Cambridge University Press

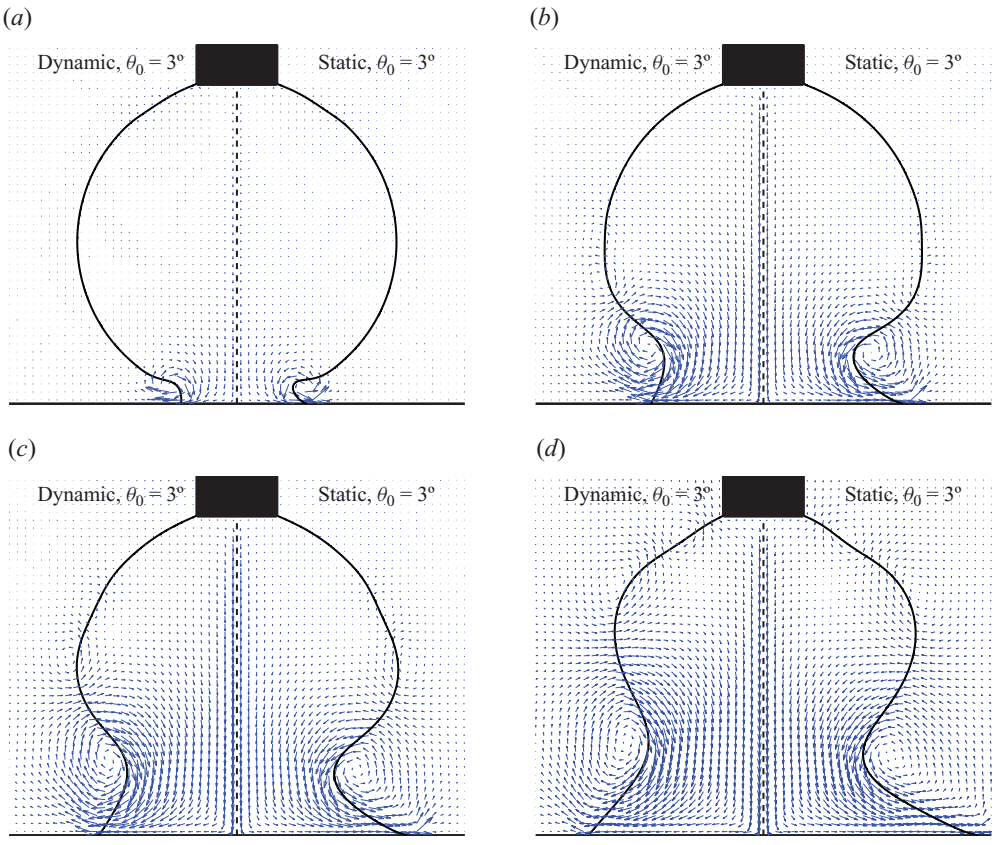


FIGURE 4. (Colour online) Numerically predicted velocity profile and droplet shape for a droplet spreading on a solid surface with an equilibrium contact angle $\theta_0 = 3^\circ$ at four snapshots in time [a: $\tau = 0.04$, b: $\tau = 0.22$, c: $\tau = 0.43$, d: $\tau = 0.63$]. The left sub-figure in each sub-part shows the result with the dynamic treatment with $D_W = 0.5$ and the right sub-figure the result using equilibrium assumption with $D_W = 0$.

3.3. *Interfacial evolution and dynamic contact angles*

Figures 4, 5, and 6 show the droplet shape and velocity vectors for a water droplet spreading on three solid surfaces with an equilibrium contact angle of $\theta_0 = [3^\circ, 43^\circ, 117^\circ]$. The left half of each panel in figures 4, 5, and 6 shows the simulations with the non-equilibrium wetting boundary condition 2.5, labelled dynamic, and the right panel the results with the local equilibrium condition 2.4, labelled static. The wording 'dynamic' and 'static' does in this context denote the contact angle boundary condition at the solid surface, which is changing in time in the former and fixed in the latter. The apparent contact angle is changing in time with both the boundary conditions.

Figure 4 shows four snapshots in time of the droplet as it spreads on a solid surface with an equilibrium contact angle $\theta_0 = 3^\circ$. In figure 4(a), the droplet has just started to wet the solid surface and has propagated about one-third of its initial radius. A larger contact angle is observed with the non-equilibrium boundary condition, left half, than with the assumption of local equilibrium, right half. Both the wetting boundary conditions produce a smooth velocity profile in the domain, being largest

https://doi.org/10.1017/jfm.2011.211 Published online by Cambridge University Press

$\theta_0 = 3^\circ$	$\tau = 0.16$	$\tau = 0.31$	$\tau = 0.47$
θ_e	71°	58°	52°
θ_s	78°	63°	52°

TABLE 1. Comparison of the experimental and numerical predicted dynamic contact angles for a solid surface with an equilibrium contact angle $\theta_0 = 3^\circ$, where θ_e is the experimental and θ_s the numerically predicted apparent dynamic contact angle.

in the vicinity of the contact line. A flow recirculation is observed with both models, with a larger local curvature predicted with the static model.

The two different models predict a somewhat different shape of the droplets interface. We see clearly that the equilibrium assumption propagates too fast over the solid surface (see figure 4*b*). A capillary wave is generated at the onset of wetting (figure 4*a*), which propagates across the droplet. This wave is visible in all of the sub-plots in figure 4. The wave propagates across the droplet before its energy is finally dissipated. By comparing these results with the experiments by Bird *et al.* (2008), we notice that the equilibrium condition over-predicts the amplitude of the capillary wave, as it relaxes faster towards its equilibrium contact angle. As the contact line moves across the solid surface, we notice two small secondary flows close to the rod (see figure 4*d*). These flow patterns are generated due to a local change in the curvature of the interface.

We have extracted the contact angle from the numerical simulations with the non-equilibrium boundary condition, as the equilibrium assumption has been found deficient. This was done by extracting the points along the zero contour for C, at several interfacial lengths in the wall-normal direction. By drawing a tangent through these points, we were able to measure the observable dynamic contact angle. These results have been compared with the experimental results from Bird *et al.* (2008) (see table 1). The apparent contact angle from Bird *et al.* (2008) has been extracted in a similar fashion as the simulation results, by drawing a tangent along the interface close to the solid surface. Here θ_e is the experimental and θ_s numerically predicted contact angles with the non-equilibrium condition. A direct match is found in time, between the measured numerical and experimental apparent dynamic contact angles, indicating that we have captured the correct value for the coefficient D_W (see table 1).

Figure 5 shows the simulation results of a water droplet that spreads on a solid surface with an equilibrium contact angle $\theta_0 = 43^\circ$. In the initial stage of the spreading (see figure 5*a*), we notice a large discrepancy between the predicted apparent contact angles with the two different wetting boundary conditions. By comparing the result using the equilibrium assumption with the experimental results by Bird *et al.* (2008), we observe that neither the contact angle nor the capillary wave is in coherence with the experiments. Good agreement is found with the local dynamic treatment. As the contact line moves in time, the difference in droplet shape predicted by the two boundary conditions becomes more pronounced (see figure 5*b*). A large flow recirculation is observed at the capillary wave (figure 5*c*) where two secondary vortices are formed as the wave approaches the needle/rod (see figure 5*d*).

A comparison between the predicted contact angle from the dynamic treatment and the experiments in time is given in table 2. In this partial wetting regime, there is a slight deviation between the experimental and numerical dynamic contact angles.

https://doi.org/10.1017/jfm.2011.211 Published online by Cambridge University Press

$\theta_0 = 43^\circ$	$\tau = 0.16$	$\tau = 0.31$	$\tau = 0.47$
θ_e	107°	99°	96°
θ_s	107°	88°	79°

TABLE 2. Comparison of the experimental and numerical predicted dynamic contact angles for a solid surface with an equilibrium contact angle $\theta_0 = 43^\circ$, where θ_e is the experimental and θ_s the numerically predicted apparent dynamic contact angle.

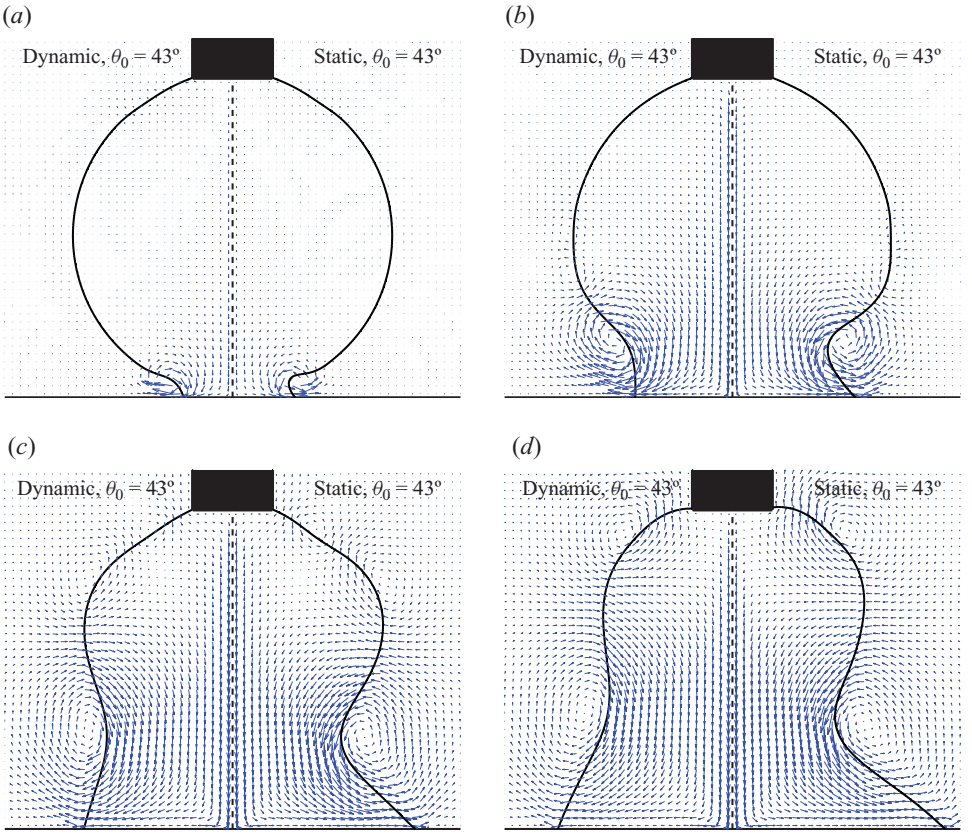


FIGURE 5. (Colour online) Numerically predicted velocity profile and droplet shape for a droplet spreading on a solid surface with an equilibrium contact angle $\theta_0 = 43^\circ$ at four snapshots in time [a: $\tau = 0.04$, b: $\tau = 0.22$, c: $\tau = 0.63$, d: $\tau = 0.82$]. The left sub-figure in each part shows the result with the dynamic treatment with $D_W = 0.7$ and the right sub-figure the result using equilibrium assumption with $D_W = 0$.

.

One explanation for the deviation can be that the coefficient D_W could be better fitted, for instance, maybe against θ_e in time instead of the spreading radius.

Figure 6 shows the droplet spreading on a solid surface with an equilibrium contact angle $\theta_0 = 117^\circ$. We notice, as also observed in figure 2(c), that the results with the non-equilibrium and equilibrium boundary conditions are hard to distinguish from each other. The flow field is almost identical with the two boundary conditions. A slight difference in the droplet shape can be seen in the initial wetting, where the contact angle is slightly larger with the dynamic treatment (see figures 6a and

https://doi.org/10.1017/jfm.2011.211 Published online by Cambridge University Press

$\theta_0 = 117^\circ$	$\tau = 0.16$	$\tau = 0.31$	$\tau = 0.47$
θ_e	147°	125°	120°
θ_s	132°	123°	120°

TABLE 3. Comparison of the experimental and numerical predicted dynamic contact angles for a solid surface with an equilibrium contact angle $\theta_0 = 117^\circ$, where θ_e is the experimental and θ_s the numerically predicted apparent dynamic contact angle.

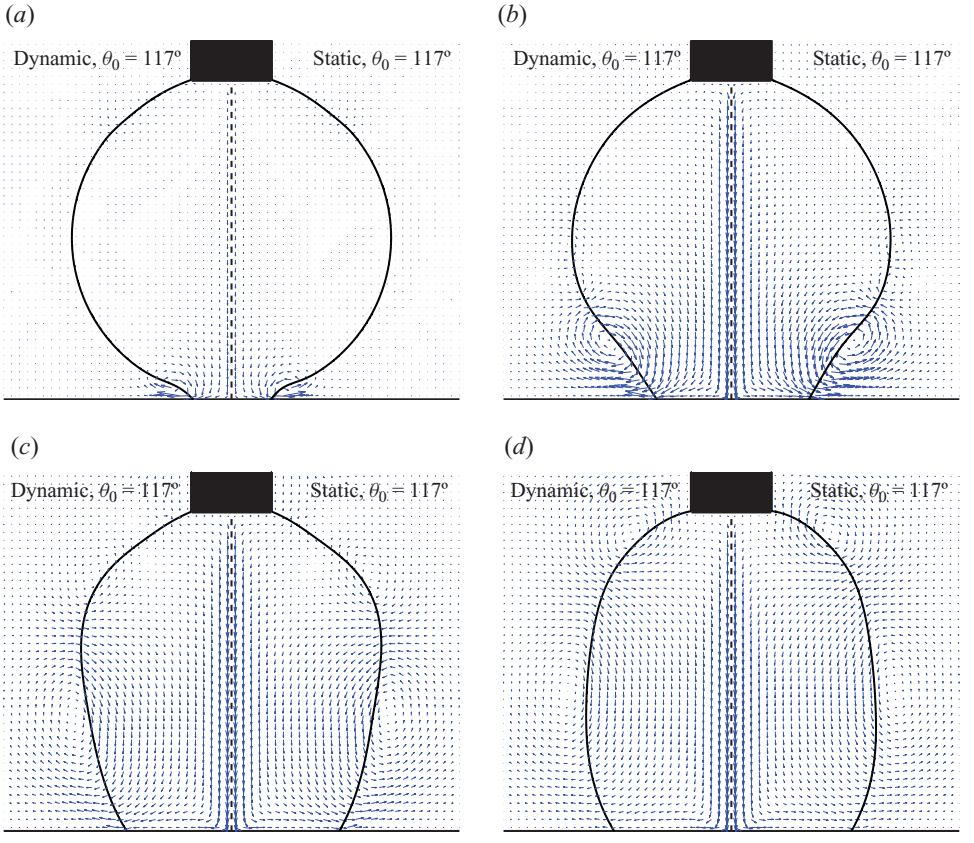


FIGURE 6. (Colour online) Numerically predicted velocity profile and droplet shape for a droplet spreading on a solid surface with an equilibrium contact angle $\theta_0 = 117^\circ$ at four snapshots in time [$a: \tau = 0.04$, $b: \tau = 0.43$, $c: \tau = 0.63$, $d: \tau = 0.82$]. The left sub-figure shows the dynamic treatment with $D_W = 0.1$ and the right sub-figure the equilibrium assumption with $D_W = 0$.

6*b*). A flow recirculation is observed as the capillary wave propagates across the droplet (figure 6*c*). In comparison with the observed wetting in figures 4 and 5, the droplet relaxes faster to its equilibrium state (see figure 6*d*). The numerically predicted dynamic contact angle gives a direct match with the experimental results from Bird *et al.* (2008) (see table 3).

3.4. *Dynamic contact angle relaxation*

Based on the results presented in figures 4, 5, and 6, it is clear that the dynamic contact angles predicted with the two boundary conditions are different. The dynamic contact

https://doi.org/10.1017/jfm.2011.211 Published online by Cambridge University Press

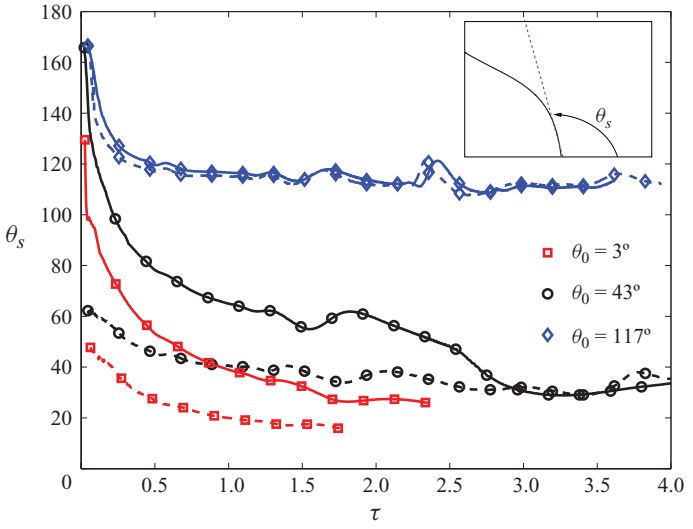


FIGURE 7. (Colour online) Temporal evolution of the dynamic contact angle evolution using the local equilibrium assumption boundary condition (dotted lines) and the non-equilibrium boundary condition (full lines). The inset in the upper right shows schematically how the contact angle is extracted along the $C = 0$ contour.

angle (θ_s) has been extracted from the simulations as it evolves in time (see figure 7). This was done by fitting a tangent through the points along the zero contour of the phase field parameter C, at a well-defined height in the wall-normal direction (z-axis). In order to say something with fidelity about the dynamic contact angle, several points are needed in the interpolation. As the droplet starts to wet the dry solid surface, the interface forms a small radius of curvature (see figures 4, 5, and 6). To extract the proper dynamic contact angle, it is important not to interpolate the contact angle at a too small or large height in the z-direction from the solid surface, since the former would produce an inaccurate result and the latter interpolate the wrong angle. The first time steps, when the radius of curvature is of the same order of magnitude as ϵ, have been disregarded, as there are not sufficient points in order to extract the contact angle with fidelity. In the first spreading phase, the radius of curvature in the foot region changes rapidly, and the interpolation height in z-direction has been taken to be equal to this radius. The wall-normal interpolation height is fixed to 15ϵ when the radius of curvature exceeds this length. The inset in figure 7 shows schematically how the dynamic contact angle is extracted. For the simulations with the equilibrium boundary condition, points closer than ϵ from the wall have been neglected when extracting the dynamic contact angle, since the equilibrium contact angle is imposed here.

One observation to be made in figure 7 is that the results obtained with the non-equilibrium boundary condition evolve towards the static contact angle (θ_0) much more slowly than with the equilibrium condition. For the cases with the non-equilibrium condition, the droplet starts to wet with a high contact angle, close to 160°. As it spreads across the surface, the contact angle changes and relaxes towards its equilibrium condition. In the initial short-time spreading, the dynamic contact angle varies rapidly.

The results with the equilibrium condition reveal that the droplet starts to wet with a contact angle that is much closer to its equilibrium angle. As the droplet

https://doi.org/10.1017/jfm.2011.211 Published online by Cambridge University Press

spreads, the dynamic contact angle varies, although not with such a span in angles as observed with the non-equilibrium condition. It seems that the temporal contact angle relaxation is much shorter with the equilibrium assumption than with the non-equilibrium condition.

The evolution of the contact angle for the surface that does not wet well ($\theta_0 = 117^\circ$), shows that there is no significant effect by using the non-equilibrium condition for this hydrophobic case. This result is in accordance with the finding in figure 2(*c*).

Figure 7 also reveals that the hydrodynamic forces present in the flow influence the evolution of the dynamic contact angle. For instance, an effect from the capillary wave can be seen in all cases around the time $\tau \sim 1.6$. This is due to the formation of a liquid neck along the symmetry axis as the droplet spreads. As the neck breaks off, two separate droplets are formed, one large on the lower surface and a small secondary droplet on the needle. This makes the droplets and the contact angles oscillate (see figure 7 for $\theta_0 = [43^\circ, 117^\circ]$ after time $\tau = 2.0$). The influence of the breakup on the dynamic contact angle is clearly observed for the case when $\theta_0 = 117^\circ$, as the surface tension contracts the droplets. Detachment from the upper wall takes place at a slightly later time, $\tau = 3.1$, with the equilibrium condition when $\theta_0 = 43^\circ$, and a different size is also predicted for the two droplets.

3.5. *Influence of the interface width and bulk diffusion*

One difficulty of the phase field method is that the interface width in practical simulations has to be taken much larger than what can be motivated physically. In the numerical experiments shown here, a Cahn number of $C_n = 10^{-2}$ has been applied. This means that in the simulations, the width of the interface is $\epsilon = 7.8\ \mu$m. Comparing the numerical and actual physical width of the interface, being of the order of a couple of Ångströms, it is clear that this numerical width does not account for the interfacial physics on length scales below ϵ. However, we will verify that the macroscopic results of the simulations are insensitive to the interface width (i.e. the Cahn number), and that this can be considered as a numerical parameter in the present context.

To show that the phase field method can capture macroscopic phenomena with accuracy, it is important to show that the simulation results are fairly independent of the width of the numerical interface. Several authors (Villanueva & Amberg (2006), Ding & Spelt (2007), Carlson, Do-Quang & Amberg (2010) and Yue *et al.* (2010) have previously demonstrated this. Since we here explore a term that has typically been neglected in phase field simulations, we have investigated the effect of C_n and Pe on the simulated wetting physics. Figure 8 shows the shape of the droplet for four simulations, with different C_n and Pe. A direct match between all the different cases is obtained for the droplet shape as well as the wetting foot-region. As these interface widths did not have any noticeable effect on the results, we are satisfied that the results are insensitive to values of C_n and Pe. Additional simulations, not presented here, with the equilibrium boundary condition show that the results were also insensitive to the C_n and Pe numbers presented in figure 8.

In the phase field context, it is thus natural to interpret Kn, appearing in the non-dimensional number $D_W = D_W^*/\mu L = Kn\,/Ag$ as being similar to the Cahn number C_n. A set of simulations were performed where the interface width was changed nearly one order of magnitude between $C_n = 2 \times 10^{-2}$ and $C_n = 0.25 \times 10^{-2}$. By changing the C_n number but retaining the same D_W, it was observed in the simulations that the contact line did not obtain the same speed. However, if the ratio D_W/C_n is held constant, the droplet shape remains nearly independent of the interface width as it

https://doi.org/10.1017/jfm.2011.211 Published online by Cambridge University Press

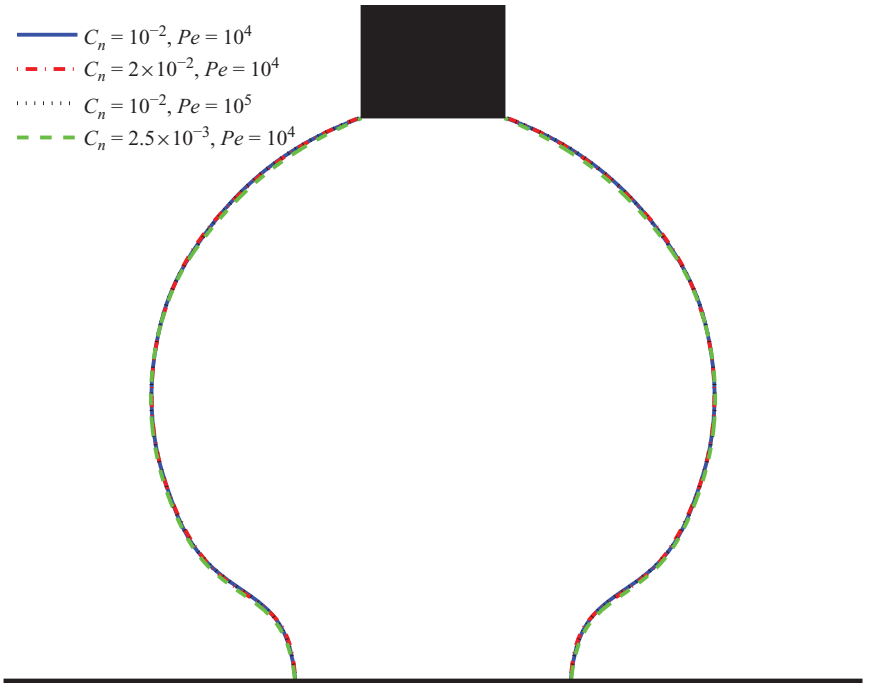


FIGURE 8. (Colour online) Effects of the interface width and bulk diffusion in the simulations for a wetting droplet on a solid surface with $\theta_0 = 43^\circ$ and $D_W = Kn/Ag = C_n/Ag$. $D_W/C_n = 140$ for the four cases shown above with different C_n and Pe.

spreads in time. This is shown in figure 8, where $D_W/C_n = 140$, indicating that it seems reasonable to interpret D_W^*/ϵ as a constant independent of the interface width.

The results for different C_n numbers are shown in figure 8, where no significant effect of the interface width was seen in the simulations, demonstrating that the use of a finite interface width can only have a very minor influence on the wetting simulations presented here. It seems for now also reasonable to interpret Ag as a non-dimensional number that is independent of the interface width. Yue *et al.* (2010) showed that to obtain convergent phase field contact line simulations with respect to the interface width, analogous to a sharp-interface limit, the simulations should satisfy $4 > \sqrt{Pe\, C_n}$ with the scaling used in the present work. Remembering that the predicted velocity in the simulations is about two orders of magnitudes less than the characteristic velocity $U = \sigma/\mu$, we notice that all simulations presented here satisfies the proposed condition for convergent results for moving contact lines, as already indicated in figure 8.

A question that naturally arises is whether the non-equilibrium boundary condition will hold in the limit of a vanishing interface width ($\epsilon \to 0$). Wang & Wang (2007) studied the asymptotic behaviour of the solution of the Cahn–Hilliard equations, by expanding the phase field variable in terms of the interface width. Near the contact line, the outer solution was shown to behave regularly, although they did not obtain a solution for the inner contact line region. They pointed out that the deviation from the equilibrium contact angle, would, indeed, depend on the inner structure of the interface at the contact line. It is in this region where the diffusive slip would act as a mechanism for the contact line movement. Based on the study by Wang &

https://doi.org/10.1017/jfm.2011.211 Published online by Cambridge University Press

Wang (2007), Yue *et al.* (2010) noted that it still remains unclear wether such a sharp interface limit exists for the Cahn–Hilliard model. However, Qian *et al.* (2004) and co-workers made a detailed comparison between the contact line motion predicted with molecular dynamics simulations and with phase field modelling. Excellent agreement was obtained for the slip profile at the nano-scale, where most parameters in the phase field equations were given directly from the molecular dynamics calculations. The non-equilibrium boundary condition, retaining a non-zero D_W, was demonstrated to be of great importance in order to obtain a matching phase field solution with the molecular dynamics simulations. They found that the contact line dissipation is an important contribution to the total dissipation at small length scales, a result that is in agreement with the findings presented in § 4.

4. Governing dissipative mechanisms in rapid dynamic wetting

To identify the different mechanisms that govern the dynamic wetting process, the different rates of dissipation have been extracted from the flow. This has been done in accordance with the methodology presented by Wang, Qian & Sheng (2008) and Qian *et al.* (2009*b*). These dissipative mechanisms are the viscous dissipation ($\dot{R}^*_\mu$), the diffusive fluxes of the chemical potential ($\dot{R}^*_D$) and the contact line relaxation at the solid surface ($\dot{R}^*_{D_W}$). However, during rapid dynamic wetting, some of the released energy is converted into bulk kinetic energy, and thus the force balance that determines the wetting speed involves the liquid inertia (Biance *et al.* 2004). Therefore, the rate of change of kinetic energy ($\dot{R}^*_\rho$) is also extracted from the flow. To identify the primary cause for resistance to spreading, the relative magnitudes of these four rates ($\dot{R}^*_\mu$, $\dot{R}^*_D$, $\dot{R}^*_{D_W}$, $\dot{R}^*_\rho$) are studied as the droplet evolves. These four contributions are scaled with the surface energy ($\dot{R}^*_\mu = \sigma UL \cdot \dot{R}_\mu$, $\dot{R}^*_D = \sigma UL \cdot \dot{R}_D$, $\dot{R}^*_{D_W} = \sigma UL \cdot \dot{R}_{D_W}$ and $\dot{R}^*_\rho = \sigma UL \cdot \dot{R}_\rho$) giving their dimensionless form

$$\left.\begin{aligned} \dot{R}_\mu &= \int_\Omega Ca\,\mu(C)\nabla\boldsymbol{u} : (\nabla\boldsymbol{u} + \nabla^T\boldsymbol{u})\,\mathrm{d}\Omega, \quad \dot{R}_D = \int_\Omega \frac{C_n}{Pe}\left(\frac{\partial\phi}{\partial t}\right)^2 \mathrm{d}\Omega, \\ \dot{R}_{D_W} &= \int_\Gamma D_W\left(\frac{\partial C}{\partial t}\right)^2 \mathrm{d}\Gamma, \quad \dot{R}_\rho = \int_\Omega \frac{Re\cdot Ca}{2}\frac{\partial\rho(C)\boldsymbol{u}^2}{\partial t}\mathrm{d}\Omega. \end{aligned}\right\} \tag{4.1}$$

Here, $\dot{R}_\mu$, $\dot{R}_D$ and $\dot{R}_\rho$ are bulk contributions (Ω), while $\dot{R}_{D_W}$ is a contribution at the solid surface (Γ).

Above, the relationship between C_n and D_W was discussed, and it was shown numerically that $D_W/C_n = 1/Ag$ is a number independent of the interface width. This indicates also that the dissipation at the contact line as it relaxes towards equilibrium, should also not depend significantly on the interface width. This can also be seen by considering here the rate of change of the order parameter C with the spreading radius (r) at the solid surface, where $\partial C/\partial t \sim (\delta C/\delta r)(\delta r/\delta t)(\sim 1/\epsilon)(\partial r/\partial t)$. This gives an estimate for the dissipation from the contact line relaxation; $\dot{R}^*_{D_W} = \int_\Gamma D^*_W(\partial C/\partial t)\mathrm{d}\Gamma \sim D^*_W[(1/\epsilon)(\partial r/\partial t)]^2(2\pi r\epsilon)$. This gives then by scaling $\dot{R}_{D_W}$ with the surface energy σUL, $\dot{R}_{D_W} \sim (D^*_W/\sigma UL)(U^2/\epsilon^2)r\epsilon \sim (D_W/C_n)(r/L) \sim (1/Ag)$. Assuming here that r is in the same order of magnitude as L, we apply the analogy as introduced above, where D_W is interpreted in terms of C_n. This shows, along with the result presented in figure 8, that the energy dissipated at the contact line does not significantly depend on C_n.

https://doi.org/10.1017/jfm.2011.211 Published online by Cambridge University Press

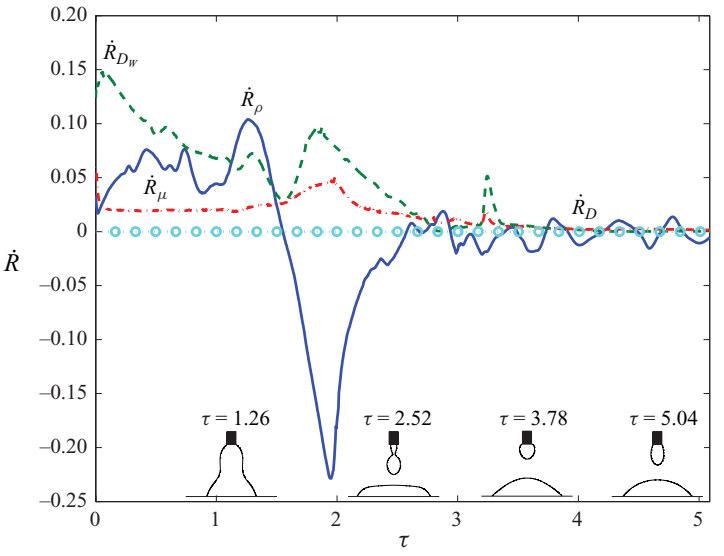


FIGURE 9. (Colour online) The rate of dissipation in time and the rate of change of kinetic energy for the spreading on a solid surface with $\theta_0 = 43°$. The full line corresponds to $\dot{R}_\rho$, dashed line $\dot{R}_{D_W}$, dashed dotted line $\dot{R}_\mu$ and the dashed line with round markers to $\dot{R}_D$. The insets in the lower part of the figure shows the droplet shape corresponding to the time given on the x-axis.

Figure 9 shows the rate of dissipation and kinetic energy for a droplet spreading on a solid surface with an equilibrium contact angle $\theta_0 = 43°$. Snapshots of the droplet shape at four different times have been placed as insets.

Initially, the droplet spreads rapidly across the solid surface and the contact line decelerates as it moves. At time $\tau = 2.0$, the extended liquid neck formed along the symmetry axis between the upper and lower wall breaks, forming a large drop on the lower solid surface and a small secondary droplet pinned at the needle tip. It is well known that the contact line dynamics influences the size of the deposited droplets (Qian *et al.* 2009*a*), thus the modelling approach presented here does not only enable a more precise prediction of the contact line spreading but also the prediction of such a droplet deposition process. The breakup time as well as the droplet sizes are different for the equilibrium and non-equilibrium boundary conditions. After breakup of the liquid neck, the droplets on the lower and upper solid surfaces oscillate as they relax into their equilibrium state (see figure 9). All these processes influence the rate of dissipation as well as the rate of change of kinetic energy (see figure 9). As the main objective here is to identify the governing mechanisms in the early rapid dynamic wetting, we will now focus on the behaviour up to the collapse of the liquid neck.

Figure 10 shows the temporal evolution of the four rates as the droplet spreads over the three different solid surfaces with $\theta_0 = [3°, 43°, 117°]$. These rates are presented until the liquid neck starts to collapse ($\tau \sim 1.5$). First, with the incipience of wetting, viscous dissipation is large as seen in all three plots in figure 10. This is in agreement with the theory proposed by Eggers *et al.* (1999), as a small cusp region is formed at the contact line. This regime has a very short time span, and is quickly replaced by another wetting regime where either the dissipation from the contact line relaxation, or the rate of change of kinetic energy dominates (see figure 10).

https://doi.org/10.1017/jfm.2011.211 Published online by Cambridge University Press

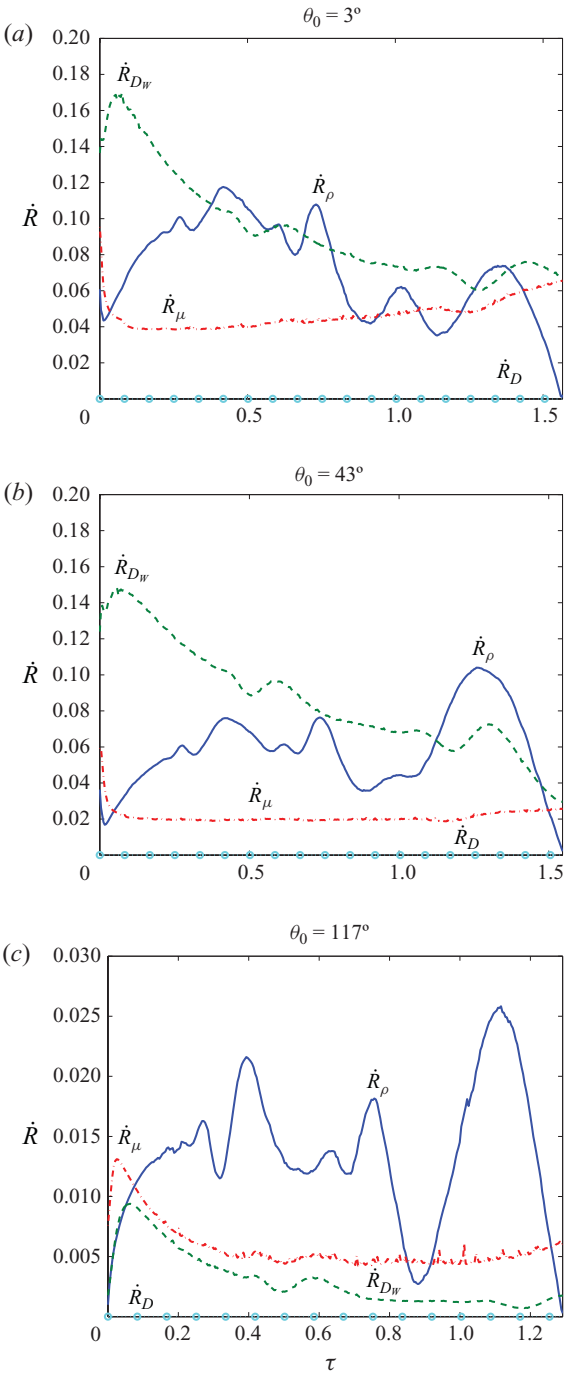


FIGURE 10. (Colour online) The rate of dissipation in time and the rate of change of kinetic energy at the early stage in the wetting process for a droplet ($L = 0.78$ mm) spreading on a solid surface with $\theta_0 = [3°, 43°, 117°$. The full line corresponds to $\dot{R}_\rho$, dashed line $\dot{R}_{D_w}$, dashed dotted line $\dot{R}_\mu$ and the dashed line with round markers to $\dot{R}_D$.

https://doi.org/10.1017/jfm.2011.211 Published online by Cambridge University Press

In figure 10(*a*), the four rates are given in time for the initial spreading on a solid surface with $\theta_0 = 3^\circ$. Initially, the viscous dissipation is large, but reduces rapidly while the dissipation from the contact line and rate of change of kinetic energy start to increase. In this early wetting, the contact line propagates with a high speed ($\sim 1\,\mathrm{m\,s^{-1}}$) across the solid surface. After the time $\tau \sim 0.05$, the dissipation from the contact line relaxation starts to decrease, and inertia becomes increasingly important. Around time $\tau \sim 0.45$, the dissipation from the contact line and the rate of change of kinetic energy balance each other. Further on, the rate of change of kinetic energy in the bulk dominates the wetting and the spreading dynamics is dominated by inertia. The contribution from the bulk diffusion of the chemical potential here is much less than the three other contributions, and has an insignificant influence on the results.

A similar scenario is observed for the initial wetting on a solid surface with $\theta_0 = 43^\circ$ (see figure 10*b*). In comparison with the results for the solid surface with $\theta_0 = 3^\circ$, it is seen that the transition between the relaxation and inertial wetting takes place at a later point in time, $\tau \sim 1.1$, as compared to $\tau \sim 0.45$ for $\theta_0 = 3^\circ$. This result is also in accordance with the values determined for the rate coefficient D_W, as D_W is found to be larger for $\theta_0 = 43^\circ$ than for $\theta_0 = 3^\circ$. The magnitudes of the different rates here are less than those observed for $\theta_0 = 3^\circ$, since the contact line moves slower.

A different picture is observed for the spreading on a solid surface that does not wet well ($\theta_0 = 117^\circ$) (see figure 10*c*). Here, viscous dissipation dominates initially, as for the two cases reported above. However, the dissipation from the contact angle relaxation seems to play a minor role in comparison with the viscous dissipation and rate of change of kinetic energy. Instead, the viscous dissipation increases in time, contrary to the observations in figures 10(*a*) and 10(*b*), and there is a transition between viscous and inertially dominated wetting around $\tau \sim 0.15$. After this transition, inertia dominates and the viscous dissipation slowly decreases.

The contact line relaxation regime is to our understanding a new dissipative mechanism, which has not previously been known to dominate the initial droplet spreading. This dissipative mechanism is believed to be a re-organization of molecules, in a type of diffusive or active process, at the contact line. In order to model rapid dynamic wetting processes with fidelity, it is important to account for this dissipative mechanism. This term, $(\sim 2\pi r \epsilon D_W (\partial C/\partial t)^2)$ resembles the term for contact line dissipation proposed by de Gennes (1985). It is also similar to the dissipation estimated from the molecular kinetics theory (de Ruijter, De Coninck & Oshanin 1999). At the present time, we are not able to determine whether these mechanisms are indeed the same, as this would require first principle studies at the molecular scale, which goes beyond the scope of the present paper. It should, however, be noted that the scaling for the spreading radius from the molecular kinetic theory $r \sim t^{1/7}$ was not recovered in the simulations, and that this regime has been shown to take place at much later time scales (De Coninck *et al.* 2001; Seveno *et al.* 2009) than what is observed in the simulations. The initial wetting regime found here, serves as an addition to the other wetting regimes that have previously been reported in the literature.

For all three cases, the viscous dissipation and the rate of change of kinetic energy balances each other several times, although at slightly different times. Later on, viscous dissipation dominates the flow, influencing the spreading rate as also seen in figure 3. The time for transition from wetting dominated by inertia to viscosity $\tau_t \sim 1.5$ (t_t) is in reasonable correspondence to the result by Biance *et al.* (2004), $\tau_t = 3.80$ ($t_t \sim$ 9.7 ms). Also, it is clear that for late time dynamics, hydrodynamic forces like the collapse of the liquid bridge and droplet oscillation influence the phenomena as illustrated in figure 9.

https://doi.org/10.1017/jfm.2011.211 Published online by Cambridge University Press

4.1. *Estimating the duration of the relaxation regime*

In view of the above, there seems to be a distinct time scale where the dissipation from the contact line dominates the wetting physics. A force balance between the capillary force generated by interface distortion and the contact line relaxation gives an estimate of the spreading radius in this regime. In this context, it is natural to interpret the contact line relaxation as a friction force at the contact line, while the capillary force is driving the flow. By following the same methodology as in Biance *et al.* (2004), it is possible to estimate the spreading radius as a function of time, assuming that the capillary force balances the contact line relaxation force as

$$\left.\begin{aligned} &2\pi r \cdot D_W^* \frac{\mathrm{d}C}{\mathrm{d}t} = 2 \cdot \pi r \sigma \\ &\sim \frac{D_W^*}{\epsilon} \frac{\mathrm{d}r}{\mathrm{d}t} \sim \sigma, \\ &r \sim \left(\frac{\sigma \epsilon}{D_W^*}\right) t. \end{aligned}\right\} \tag{4.2}$$

Equation (4.2) along with the estimate for the spreading radius for inertial-driven wetting Biance *et al.* (2004) $r \sim (\sigma L/\rho)^{1/4} t^{1/2}$, gives then a characteristic time for the transition between the relaxation and the inertial regime $t_t \sim ((\sigma L/\rho)^{1/4}/(\sigma/\epsilon D_W^*))^2$.

By introducing the material properties for the density, rate coefficient, length and surface tension coefficient, the duration of the wetting is found to be dominated by the contact line relaxation, and a distinct time for the wetting transition between the inertial and the contact line relaxation regime is obtained. For the three cases reported above, the transitional time (t_t) should be $t_t = [0.44, 0.88, 0.018]$ms or $\tau_t = [0.18, 0.34, 0.007]$ for $\theta_0 = [3^\circ, 43^\circ, 117^\circ]$. These results are in good agreement with the numerically predicted transitional time. The transition time for $\theta_0 = 117^\circ$ is very short, possibly within the viscous cusp region, where viscosity dominates. The latter is supported by the numerical result, presented in figure 10(*c*).

5. Conclusion

A phase field modelling approach for rapid dynamic wetting is presented, where the dissipative mechanisms that dictate the evolution are identified. It is shown that it is crucial that the mathematical modelling accounts for non-equilibrium effects at the contact line. In particular, we demonstrate that a contact line model assuming local equilibrium will be deficient. A coefficient that appears in the non-equilibrium boundary condition is interpreted as allowing for a diffusive reorganization at the contact line. This coefficient thus represents the molecular processes of the contact line, and parameterizes their influence on the macroscopic spreading rate. At the present time, we could only get the order of magnitude of this coefficient from independent experimental data.

Rapid spontaneous spreading of liquid droplets on solid surfaces with different degrees of wettability was studied numerically. A direct match with the temporal evolution of the experimental spreading radius by Bird *et al.* (2008) was obtained. Good agreement was also found between the numerical and experimental apparent dynamic contact angles in time. The results presented here were found not to depend significantly on the bulk diffusion or interface width. As a consequence, meaningful simulation results can be obtained by using interface widths that are much larger than what can be physically motivated.

https://doi.org/10.1017/jfm.2011.211 Published online by Cambridge University Press

By tracing the rate of dissipation and the rate of change of the kinetic energy, we found a new wetting regime, where the dissipation from the contact line relaxation dominates. This is to our knowledge the first time that this dissipative mechanism is found to dominate a dynamic wetting process. This serves as a new wetting regime complementing the regimes previously reported in the literature. The three wetting regimes predicted from hydrodynamic theory (Eggers *et al.* 1999; Biance *et al.* 2004; Bird *et al.* 2008) were also identified in the simulations. A reasonably good match was found for the time of transition from inertial to viscously dominated wetting between the simulations and the theory proposed by Biance *et al.* (2004).

Finally, a spreading law for the relaxation regime was derived based on a balance between the capillary force and the contact line friction. This along with the spreading law for inertially dominated wetting (Biance *et al.* 2004) yields as a distinct criterion for the transition between wetting dominated by contact line relaxation and inertia. The transitional times found in the simulations are in good agreement with the theoretical predictions.

Funding from the Swedish Research council (VR) through the Linnè Flow Center is acknowledged.

REFERENCES

Aarts, D. G. A. L., Lekkerkerker, H. N. W., Guo, H., Wegdam, G. H. & Bonn, D. 2005 Hydrodynamics of droplet coalescence. *Phys. Rev. Lett.* **95** (16), 164503.

Amberg, G., Tonhardt, R. & Winkler, C. 1999 Finite element simulations using symbolic computing. *Maths. Comput. Simul.* **49** (4–5), 257–274.

Biance, A. L., Clanet, C. & Quere, D. 2004 First steps in the spreading of a liquid droplet. *Phys. Rev.* E **69** (1), 016301.

Bird, J. C., Mandre, S. & Stone, H. A. 2008 Short-time dynamics of partial wetting. *Phys. Rev. Lett.* **100** (23), 234501.

Blake, T. D. 2006 The physics of moving wetting lines. *J. Colloid and Interface Sci.* **299**, 1–13.

Blake, T. D. & Haynes, J. M. 1969 Kinetics of liquid/liquid displacement. *J. Colloid and Interface Sci.* **30** (3), 421–423.

Blake, T. D. & Shikhmurzaev, Y. D. 2002 Dynamic wetting by liquids of different viscosity. *J. Colloid and Interface Sci.* **253** (1), 196–202.

Bonn, D., Eggers, J., Indekeu, J., Meunier, J. & Rolley, E. 2009 Wetting and spreading. *Rev. Mod. Phys.* **81** (2), 739–805.

Briant, A. J. & Yeomans, J. M. 2004 Lattice Boltzmann simulations of contact line motion. Part II. Binary fluids. *Phys. Rev.* E **69** (3), 031603.

Cahn, J. W. & Hilliard, J. E. 1958 Free energy of a nonuniform system. I. Interfacial free energy. *J. Chem. Phys.* **28** (2), 258–267.

Carlson, A., Do-Quang, M. & A., Gustav 2009 Modeling of dynamic wetting far from equilibrium. *Phys. Fluids* **21** (12), 12170 (1–4).

Carlson, A., Do-Quang, M. & Amberg, G. 2010 Droplet dynamics in a bifurcating channel. *Intl J. Multiphase Flow*.

Courbin, L., Bird, J. C. & Stone, H. A. 2009 Dynamics of wetting: From inertial spreading to viscous imbibtion. *J. Physics, Condens. Matter* **21**, 464127.

Cox, R. G. 1986 The dynamics of the spreading of liquids on a solid surface. Part 1. Visocus flow. *J. Fluid Mech.* **168**, 169–194.

De Coninck, J., de Ruijter, M. J. & Voue, M. 2001 Dynamics of wetting. *Curr. Opin. Colloid Interface Sci.* **6** (1), 49–53.

Ding, H. & Spelt, P. D. M. 2007 Wetting condition in diffuse interface simulations of contact line motion. *Phys. Rev.* E **75** (4), 046708.

https://doi.org/10.1017/jfm.2011.211 Published online by Cambridge University Press

Do-Quang, M. & Amberg, G. 2009 The splash of a solid sphere impacting on a liquid surface: Numerical simulation of the influence of wetting. *Phys. Fluids* **21** (2), 022102.

Do-Quang, M., Villanueva, W., Singer-Loginova, I. & Amberg, G. 2007 Parallel adaptive computation of some time-dependent materials-related microstructural problems. *Bull. Polish Acad. Sci. – Tech. Sci* **55** (2), 229–237.

Drelich, J. & Chibowska, D. 2005 Spreading kinetics of water drops on self-assembled monolayers of thiols: Significance of inertial effects. *Langmuir* **21** (17), 7733–7738.

Eggers, J. & Evans, R. 2004 Comment on 'Dynamic wetting by liquids of different viscosity,' by T. D. Blake and Y. D. Shikhmurzaev. *J. Colloid and Interface Sci.* **280** (2), 537–538.

Eggers, J., Lister, J. R. & Stone, H. A. 1999 Coalescence of liquid drops. *J. Fluid Mech.* **401**, 293–310.

de Gennes, P. G. 1985 Wetting – statics and dynamics. *Rev. Mod. Phys.* **57** (3), 827–863.

Glasstone, S., Laidler, K. J. & Eyring, H. J. 1941 *The Theory of Rate Processes.* McGraw-Hill.

Guermond, J. L. & Quartapelle, L. 2000 A projection FEM for variable density incompressible flows. *J. Comput. Phys.* **165** (1), 167–188.

Hoffman, R. L. 1975 A study of the advancing interface. I. Interface shape in liquid–gas systems. *J. Colloid and Interface Sci.* **50** (2), 228–241.

Huh, C. & Scriven, L. E. 1971 Hydrodynamic model of steady movement of a solid/liquid/fluid contact line. *J. Colloid and Interface Sci.* **35** (1), 85–101.

Jacqmin, D. 1999 Calculation of two-phase Navier–Stokes flows using phase-field modeling. *J. Comput. Phys.* **155** (1), 96–127.

Jacqmin, D. 2000 Contact-line dynamics of a diffuse fluid interface. *J. Fluid Mech.* **402**, 57–88.

Matsumoto, S., Maruyama, S. & Saruwatari, H. 1995 A molecular dynamics simulation of a liquid droplet on a solid surface. In *Proc. ASME/JSME Therm. Eng. Conf*, Maui, Hawaii.

Ngan, C. G., Dussan, V. & Elizabeth, B. 1982 On the nature of the dynamic contact angle: an experimental study. *J. Fluid Mech.* **118**, 27–40.

Petrov, P. G. & Petrov, J. G. 1992 A combined molecular-hydrodynamic approach to wetting kinetics. *Langmuir* **8** (7), 1762–1767.

Qian, B., Loureiro, M., Gagnon, D. A., Tripathi, A. & Breuer, K. S. 2009*a* Micron-scale droplet deposition on a hydrophobic surface using a retreating syringe. *Phys. Rev. Lett.* **102** (16), 164502.

Qian, T. Z., Wang, X. P. & Sheng, P. 2003 Molecular scale contact line hydrodynamics of immiscible flows. *Phys. Rev.* E **68** (1), 016306.

Qian, T. Z., Wang, X. P. & Sheng, P. 2004 Power-law slip profile of the moving contact line in two-phase immiscible flows. *Phys. Rev. Lett.* **93** (9), 094501.

Qian, T. Z., Wang, X. P. & Sheng, P. 2006*a* Molecular hydrodynamics of the moving contact line in two-phase immiscible flows. *Commun. Comput. Phys.* **1** (1), 1–52.

Qian, T. Z., Wang, X. P. & Sheng, P. 2006*b* A variational approach to moving contact line hydrodynamics. *J. Fluid Mech.* **564**, 333–360.

Qian, T. Z., Wu, C. M., Lei, S. L., Wang, X. P. & Sheng, P. 2009*b* Modeling and simulations for molecular scale hydrodynamics of the moving contact line in immiscible two-phase flows. *J. Phys., Condens. Matter* **21** (46), 464119.

Ren, W. Q. & E, W. N. 2007 Boundary conditions for the moving contact line problem. *Phys. Fluids* **19** (2), 022101.

de Ruijter, M. J., De Coninck, J. & Oshanin, G. 1999 Droplet spreading: Partial wetting regime revisited. *Langmuir* **15** (6), 2209–2216.

Saiz, E. & Tomsia, A. P. 2004 Atomic dynamics and Marangoni films during liquid–metal spreading. *Nat. Mater.* **3** (12), 903–909.

Seveno, D., Vaillant, A., Rioboo, R., Adao, H., Conti, J. & De Coninck, J. 2009 Dynamics of wetting revisited. *Langmuir* **25** (22), 13034–13044.

Shikhmurzaev, Y. D. & Blake, T. D. 2004 Response to the comment on [J. Colloid Interface Sci. 253 (2002) 196] by J. Eggers and R. Evans. *J. Colloid and Interface Sci.* **280** (2), 539–541.

Tanner, L. H. 1979 The spreading of silicone oil drops on horizontal surfaces. *J. Phys.* D **12**, 1473–1484.

Villanueva, W. & Amberg, G. 2006 Some generic capillary-driven flows. *Intl J. Multiphase Flow* **32** (9), 1072–1086.

https://doi.org/10.1017/jfm.2011.211 Published online by Cambridge University Press

Voinov, O. V. 1976 Hydrodynamics of wetting. *Izvestiya Akademii Nauk SSSP, Makhanika Zhidkosti i Gaza* **5** (76–84).

Wang, X. P., Qian, T. Z. & Sheng, P. 2008 Moving contact line on chemically patterned surfaces. *J. Fluid Mech.* **605**, 59–78.

Wang, X. P. & Wang, Y. G. 2007 The sharp interface limit of a phase field model for moving contact line problem. *Meth. Appl. Anal.* **14** (3), 287–294.

Yue, P., Zhou, C. & Feng, J. J. 2010 Sharp-interface limit of the Cahn–Hilliard model for moving contact lines. *J. Fluid Mech.* **645** (1), 279–294.

https://doi.org/10.1017/jfm.2011.211 Published online by Cambridge University Press